

PandaX-xT – a Deep Underground Multi-ten-tonne Liquid Xenon Observatory

Abdusalam Abdukerim², Zihao Bo², Wei Chen², Xun Chen^{1,3}, Chen Cheng⁴, Zhaokan Cheng⁵, Xiangyi Cui¹, Yingjie Fan⁶, Deqing Fang⁷, Lisheng Geng^{8,9,10,11}, Karl Giboni², Linhui Gu², Xunan Guo⁸, Xuyuan Guo¹², Zhichao Guo⁸, Chencheng Han¹, Ke Han², Changda He², Jinrong He¹⁰, Di Huang², Junting Huang², Zhou Huang², Ruquan Hou³, Yu Hou¹³, Xiangdong Ji¹⁴, Yonglin Ju¹³, Chenxiang Li², Jiafu Li⁴, Mingchuan Li¹², Shuaijie Li^{12,1}, Tao Li⁵, Qing Lin^{15,16}, Jianglai Liu^{*1,2,3}, Congcong Lu¹³, Xiaoying Lu^{17,18}, Lingyin Luo¹⁹, Yunyang Luo¹⁶, Wenbo Ma², Yugang Ma⁷, Yajun Mao¹⁹, Yue Meng^{2,3}, Xuyang Ning², Binyu Pang^{17,18}, Ningchun Qi¹², Zhicheng Qian², Xiangxiang Ren^{17,18}, Nasir Shaheed^{17,18}, Xiaofeng Shang², Xiyuan Shao²⁰, Guofang Shen⁸, Lin Si², Wenliang Sun¹², Yi Tao^{2,3}, Anqing Wang^{17,18}, Meng Wang^{17,18}, Qiuhong Wang⁷, Shaobo Wang^{2,21}, Siguang Wang¹⁹, Wei Wang^{5,4}, Xiuli Wang¹³, Xu Wang², Zhou Wang^{2,3,1}, Yuehuan Wei⁵, Mengmeng Wu⁴, Weihao Wu², Yuan Wu², Mengjiao Xiao², Xiang Xiao⁴, Binbin Yan¹, Xiyu Yan²², Yong Yang², Chunxu Yu²⁰, Ying Yuan², Zhe Yuan⁷, Youhui Yun², Xinning Zeng², Minzhen Zhang², Peng Zhang¹², Shibo Zhang², Shu Zhang⁴, Tao Zhang^{2,3}, Wei Zhang¹, Yang Zhang^{17,18}, Yingxin Zhang^{17,18}, Yuanyuan Zhang¹, Li Zhao^{2,3}, Jifang Zhou¹², Ning Zhou^{2,3}, Xiaopeng Zhou⁸, Yong Zhou¹⁰, Yubo Zhou², and Zhizhen Zhou²

(PandaX Collaboration)

¹New Cornerstone Science Laboratory, Tsung-Dao Lee Institute, Shanghai Jiao Tong University, Shanghai, 200240, China

²School of Physics and Astronomy, Shanghai Jiao Tong University, Key Laboratory for Particle Astrophysics and Cosmology (MoE), Shanghai Key Laboratory for Particle Physics and Cosmology, Shanghai 200240, China

³Shanghai Jiao Tong University Sichuan Research Institute, Chengdu 610213, China

⁴School of Physics, Sun Yat-Sen University, Guangzhou 510275, China

⁵Sino-French Institute of Nuclear Engineering and Technology, Sun Yat-Sen University, Zhuhai, 519082, China

⁶Department of Physics, Yantai University, Yantai 264005, China

⁷Key Laboratory of Nuclear Physics and Ion-beam Application (MOE), Institute of Modern Physics, Fudan University, Shanghai 200433, China

⁸School of Physics, Beihang University, Beijing 102206, China

⁹Peng Huanwu Collaborative Center for Research and Education, Beihang University, Beijing 100191, China

¹⁰Beijing Key Laboratory of Advanced Nuclear Materials and Physics, Beihang University, Beijing 102206, China

¹¹Southern Center for Nuclear-Science Theory (SCNT), Institute of Modern Physics, Chinese Academy of Sciences, Huizhou 516000, China

¹²Yalong River Hydropower Development Company, Ltd., Chengdu 610051, China

¹³School of Mechanical Engineering, Shanghai Jiao Tong University, Shanghai 200240, China

¹⁴Department of Physics, University of Maryland, College Park, Maryland 20742, USA

¹⁵State Key Laboratory of Particle Detection and Electronics, University of Science and Technology of China, Hefei 230026, China

¹⁶Department of Modern Physics, University of Science and Technology of China, Hefei 230026, China

¹⁷Research Center for Particle Science and Technology, Institute of Frontier and Interdisciplinary Science, Shandong University, Qingdao 266237, Shandong, China

¹⁸Key Laboratory of Particle Physics and Particle Irradiation of Ministry of Education, Shandong University, Qingdao 266237, Shandong, China

¹⁹State Key Laboratory of Nuclear Physics and Technology, School of Physics, Peking University, Beijing 100871, China

²⁰School of Physics, Nankai University, Tianjin 300071, China

²¹SJTU Paris Elite Institute of Technology, Shanghai Jiao Tong University, Shanghai, 200240, China

²²School of Physics and Astronomy, Sun Yat-Sen University, Zhuhai, 519082, China

October 31, 2024

Abstract

We propose a major upgrade to the existing PandaX-4T experiment at the China Jinping Underground Laboratory. The new experiment, PandaX-xT, will be a multi-ten-tonne liquid xenon, ultra-low background, and general-purpose observatory. The full-scaled PandaX-xT contains a 43-tonne liquid xenon active target. Such an experiment will significantly advance our fundamental understanding of particle physics and astrophysics. The sensitivity of dark matter direct detection will be improved by nearly two orders of magnitude compared to the current best limits, approaching the so-called “neutrino floor” for a dark matter mass above $10 \text{ GeV}/c^2$, providing a key test to the Weakly Interacting Massive Particle paradigm. By searching for the neutrinoless double beta decay of ^{136}Xe isotope in the detector, the effective Majorana neutrino mass can be measured to a $[10 - 41] \text{ meV}/c^2$ sensitivity, providing a key test to the Dirac/Majorana nature of neutrinos. Astrophysical neutrinos and other ultra-rare interactions can also be measured and searched for with an unprecedented background level, opening up new windows of discovery. Depending on the findings, PandaX-xT will seek the next stage upgrade utilizing isotopic separation of natural xenon.

1 Introduction

Dark matter (DM) and neutrinos are crucial matter ingredients in the Universe, both playing key roles in the evolution of the Universe and the formation of galactic structures. However, the nature of the dark matter remains unknown. Some fundamental properties of neutrinos are also elusive. One of the leading candidates of DM is the so-called “Weakly Interacting Massive Particles” (WIMPs). They emerge naturally from various extensions of the Standard Model of particle physics, for example, Supersymmetry, and can reproduce the observed DM relic density without fine-tuning [1, 2]. In 1985, inspired by the experimental development in searching for coherent neutrino-nucleus scatterings, Goodman and Witten proposed to use similar detectors to search for rare collisions between DM particles and atomic nuclei [3]. This experimental approach, known as the DM direct detection, has been carried out around the globe for nearly forty years (see, for example, Refs. [4, 5, 6, 7, 8, 9] and references therein). In recent decades, the dual-phase xenon time projection chamber (TPC) has emerged as a leading experimental technique and made very fast progress on the detection sensitivity to DM-nucleon interactions, covering a wide range of parameter space for a DM mass greater than a few GeV/c^2 . Three large experimental collaborations, PandaX [10], XENON [11], and LZ [12] have now all entered the multi-tonne-target stage. Yet, no clear DM signals have been observed. Ultimately, the sensitivity of DM direct detection will be limited by the neutrino background from the coherent scatterings of solar and atmospheric neutrinos with nuclei, known as the “neutrino floor” [13] or “neutrino fog” [14]. It is worth noting that once the neutrino floor is reached, the xenon detector is also a sensitive probe of neutrino interactions, which offers new physics opportunities on its own.

The neutrino can be either different from or the same as its own anti-particle, known as the Dirac or Majorana fermion, respectively [15]. The Majorana nature of the neutrino would offer a natural explanation for the smallness of the neutrino mass via the so-called Seesaw mechanism [16, 17, 18, 19, 20], and may also be connected to the matter-antimatter asymmetry in the Universe through Leptogenesis [21]. It has been long realized that if neutrinos are Majorana fermions, an ultra-rare nuclear decay known as the Neutrinoless Double Beta Decay (NLDBD) will happen [22]. NLDBD experiments can probe the effective Majorana neutrino mass ($m_{\beta\beta}$), a linear combination of three neutrino mass eigenvalues therefore dependent on the neutrino mass ordering (MO) [23]. Over the years, quite many NLDBD experiments have been carried out. The most recent ones search for NLDBD with the sensitivity of $m_{\beta\beta}$ at $\mathcal{O}(100) \text{ meV}$ [24, 25, 26, 27, 28, 29, 30]. KamLAND-Zen, which uses 800 kg of enriched ^{136}Xe , has recently produced the best upper limit on $m_{\beta\beta}$ of $[36 - 156] \text{ meV}/c^2$ [30]. Some future experiments, such

*spokesperson: jianglai.liu@sjtu.edu.cn

as nEXO (^{136}Xe) [31], KamLAND2-ZEN (^{136}Xe) [32], LEGEND (^{76}Ge) [33], CDEX-300 ν (^{76}Ge) [34], JUNO-DBD ($^{130}\text{Te}/^{136}\text{Xe}$) [35], CUPID (^{100}Mo) [36], are aiming at a sensitivity of 15 meV/ c^2 or better, to fully cover the parameter space corresponding to the so-called inverted neutrino MO.

The DM direct detection and NLDBD experiments both pursue extremely low background and share similar detection techniques. However, due to vastly different energy regions and signal characteristics, and that NLDBD experiments normally require enriched isotopes and emphasize the energy resolution in the MeV region, the two types of experiments are mostly developed in parallel. Recently, securing large amounts of enriched isotopes for NLDBD searches has become a major challenge. On the other hand, XENON and LZ have demonstrated to achieve a sub-percent energy resolution around 2.5 MeV, the Q -value of ^{136}Xe NLDBD [37, 38]. Consequently, the approach of using a large natural xenon detector (containing $\sim 8.9\%$ ^{136}Xe) to simultaneously pursue both avenues becomes increasingly attractive [39, 40, 41].

The China Jinping underground Laboratory (CJPL), located in Sichuan Province, China, with an overburden of 2,400 m, is currently the deepest underground laboratory in the world [42]. The extreme depth provides superb shielding to cosmic rays and related background, ideal for the experimental studies of DM and neutrinos. Two main experiments, the PandaX [43, 44] and CDEX [45, 46, 47], have been developing staged research programs on the DM and neutrinos at CJPL since 2009. The previous two generations of PandaX featuring a 120 kg (PandaX-I) and 580 kg (PandaX-II) liquid xenon (LXe) TPC, respectively, had produced competitive results in dark matter search [48, 49, 50], as well as in neutrino studies [51]. PandaX-4T, with a sensitive target of 4 tonnes of LXe, is under operation in the newly expanded CJPL-II [52]. With only the commissioning data, it produced leading constraints to DM-nucleon and DM-electron interactions [10, 53, 54, 55] and the electromagnetic properties of the DM [56, 57], and made a precise determination of the two-neutrino double beta decay (DBD) lifetime of ^{136}Xe [58] and the best lower limits on the lifetimes of DBD and NLDBD of ^{134}Xe [59]. As CJPL-II is being transformed into a general-purpose National Major Scientific Facility in China, we propose a next-generation experiment, PandaX-xT, with a multi-ten-tonne active target, strategically combining the DM and NLDBD efforts. When reaching its full scale, PandaX-xT is envisioned to contain 47 tonnes of natural xenon, of which 43 tonnes function as the active target. The main scientific objectives of PandaX-xT include, but are not limited to:

1. Searching for DM-nucleon interactions with sensitivity at 90% C.L. down to the neutrino floor, a key test on the WIMP DM paradigm;
2. A stringent test on the Majorana nature of neutrinos using the NLDBD of ^{136}Xe , covering most of the parameter space for inverted neutrino MO;
3. Detecting low-energy neutrinos from the Sun and other astrophysical origins, and searching for ultra-rare new physics signals in general.

In the rest of this paper, we shall discuss the conceptual design of PandaX-xT, the background projections in different energy regions, and its scientific potential.

2 Conceptual Design of PandaX-xT

The overall design of the PandaX-xT is shown in Fig. 1, reusing most of the existing lab infrastructure from PandaX-4T. The LXe detector is located in the center of an outer ultrapure water veto (OVETO). To achieve an extremely low background environment, the LXe cryostat in which the TPC is placed is made with a thin-walled (~ 3 mm) ultrapure copper inner vessel (IV), with a double-walled vacuum insulated low background titanium outer vessel (OV). In between the IV and OV, a low-temperature liquid scintillator (LS) volume is pressurized to balance the internal pressure of the IV, and also acts as an anti-coincidence detector to suppress the background (IVETO). The layout of the TPC, IVETO, and OV is shown in Fig. 2. To satisfy the needs of detecting DM, NLDBD, and astroparticle neutrinos, PandaX-xT is required to have an effective energy range between 100 eV and 10 MeV, an energy resolution of $\sigma/E < 1\%$ at 2.5 MeV, and a sub-cm vertex resolution. The major detector components of PandaX-xT and key design features will be discussed below.

The OVETO utilizes the passive water shielding in PandaX-4T, contained in a stainless steel (SS) tank with a total volume of 900 m³ (13 m height and 10 m diameter). The radioactivity from the experimental hall is shielded by the water to a negligible level. The radioactivity of the water was measured during the PandaX-4T operation to be ~ 10 $\mu\text{Bq/kg}$ for ^{238}U , ^{232}Th , ^{40}K and ^{222}Rn , leading also to a negligible background contribution [60, 61]. We plan to instrument the water shielding with two layers of 8-inch PMTs, separated by Tyvek foil as optical reflectors. The inner layer serves as a neutron veto with some gamma vetoing capability. The inner PMTs will be mounted on the surface of a cylinder surrounding and looking toward the liquid xenon detector, providing a photocathode coverage of $\sim 10\%$. The neutrons are tagged by the 2.2 MeV gamma rays from hydrogen captures, and the tagging efficiency is estimated by a Geant4 [62] simulation to be about 70% assuming a trigger threshold of 5 fired PMTs.

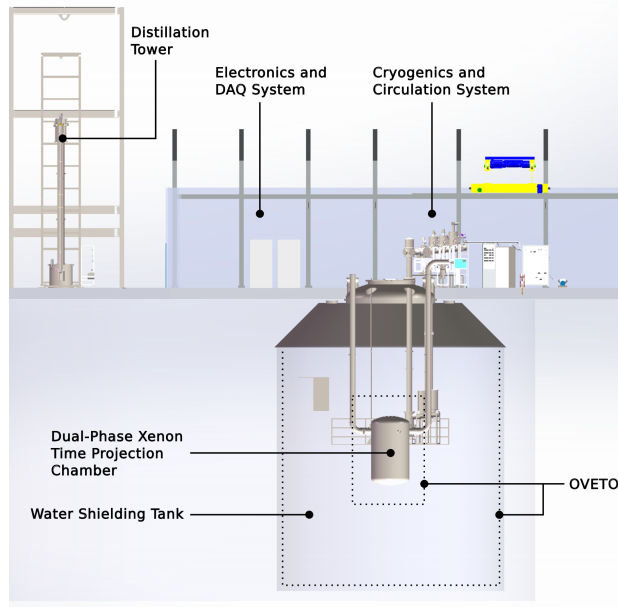


Figure 1: Schematics of the overall layout of PandaX-xT.

At a later stage, to increase the light yield and thereby neutron tagging efficiency, we plan to blend about 5% LS in the water using water-based liquid scintillator (WbLS). The WbLS technology, together with its potential applications, have been studied over a decade in the field [63, 64, 65, 66, 67, 68]. The 5% blending ratio is a modest assumption that is also used in the simulation of THEIA, a proposed neutrino detector using WbLS [66]. We have also been experimenting different WbLS formulas for our application.

The outer layer consists of PMTs mounted on the wall of the cylindrical water container in a sparser arrangement compared to the inner layer, providing a very high efficiency in vetoing muons and muon-induced hadronic showers. Additionally, with more PMTs, we are planning to further expand the OVETO from the 0.9 kton water tank to the water pit in which the water tank is situated. The pit is going to be filled with 4.5 kton ultra-pure water, about a tenth of the mass of the Super-K detector. Super-K detects about 10 atmospheric neutrino events per day above 100 MeV [69]. By a simple scaling, we expect about one atmospheric neutrino event per day in the expanded OVETO, although the event rate will also be affected by other factors, such as the detection efficiency and the low latitude of the detector location [70]. Such in-situ measurement will provide data to potentially constrain the atmospheric neutrino modeling at the Jinping site.

The IVETO is a layer of 0.5 m thick LS instrumented with plastic wavelength shifting (WLS) fibers coupled to an array of photosensors. The LS will be under the liquid xenon temperature, which is about -100°C . The neutron capture signals in LS or partial energy deposition from gamma rays from internal materials will be tagged to provide an effective veto for the otherwise candidate events happening in the TPC. The design is still under R&D with open outcome, but is based on several existing technologies:

- The cold liquid scintillator under -50°C has been successfully developed for the TAO experiment [71, 72]. The cocktail is a LAB-based LS mixed with PPO, bis-MSB and ethanol. We are exploring the LS performance under -100°C , starting with the recipe used in TAO.
- The use of the WLS fibers to collect and shift the wavelength of the scintillation photons is a widely-used approach (see, e.g., Refs. [73, 74]). Importantly, the fibers can work stably under cryogenic temperature as shown in GERDA experiment where the fibers were immersed in liquid argon [75].
- At the LXe temperature, without trying to remove the water content in the LS as in TAO, it was observed that the LAB-based LS stays as a thick translucent fluid. As already demonstrated by the LiquidO project [76], opaque LS in fact helps the photon collection by the WLS fibers, due to localized scintillation photons as a result of a short scattering length.
- The LS can provide pressure balance and additional shielding for the copper inner cryostat. The basic idea was pioneered by EXO-200, where cryogenic fluid (HFE-7000) is filled between the cryostat vessel and the LXe vessel [77]. The pressure balance allows a significant reduction in the thickness of the copper cryostat to minimize the radioactive background. For PandaX-xT, we are adding the veto functionality by using the cold LS instead of cryogenic fluid.

Based on our optical simulation, assuming a typical light yield of 10,000 photons per MeV for the LS at LXe temperature, and a Mie scattering length (which determines the opaqueness of the LS) of 3 mm, a 200 keV energy deposition with the distance to fiber of 5 mm gives approximately 5 PEs at the readout

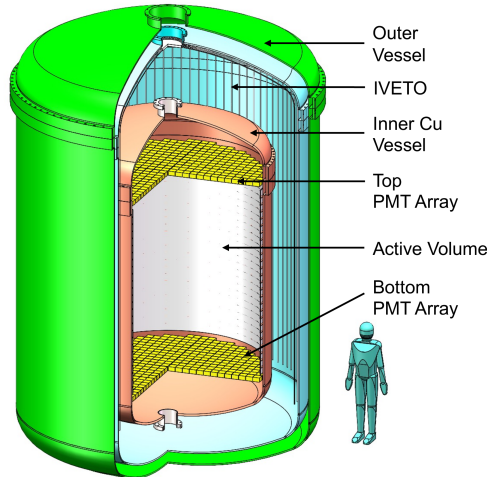


Figure 2: Schematic drawing of the conceptual design of the PandaX-xT cryostat and TPC. The IVETO region is 0.5 m thick between the IV and OV. Extra space above the IV is reserved for top feedthroughs and xenon tubes.

with an avalanche photodiode. Therefore, in this study, 200 keV is assumed as the threshold for the IVETO. The veto efficiency for low-energy neutron background events is estimated to be about 86% via a simulation (Sec. 3). The neutron background levels presented in later Table 1 assume the application of IVETO, and they are small even without the IVETO. However, IVETO will be an important insurance if the actual levels of radioactivities are worse than the specifications (see Sec. 3). In addition, IVETO will serve as a pressure balancer for the thin-walled Cu vessel (allowing for reducing the vessel’s material) and a thermal buffer for the TPC.

The cryostat system holds the liquid xenon target and TPC at 178 K, with a maximum working pressure of 0.35 MPa, while preventing contamination by external radioactivity and electronegative impurity. To meet the low background requirements of the PandaX detector, as mentioned earlier the IV is made with a thin-walled oxygen-free copper container with a diameter of ~ 2.65 m and a total height of ~ 4 m containing the liquid xenon. The copper vessel thickness is kept thin to minimize its mass and radioactivity. The OV is a double-walled vacuum-insulated titanium vessel with an outer (inner) diameter of ~ 4 m (3.5 m) and an outer (inner) height of ~ 6 m (5 m). In between the IV and OV is a 0.5 m-thick LS IVETO region, with its pressure balanced with the liquid xenon, so the actual pressure is held by the OV. Special care has to be taken in the copper vessel design due to the non-uniform pressure caused by the LXe height, as well as in the control of pressure during the filling and emptying of the detector. The LXe TPC defines the active volume of the detector. In the conceptual design, the PandaX-xT TPC is 2.55 meters in diameter and 2.95 meters in height. It is enclosed by large, photon-transparent electrodes (the cathode, gate, and anode), which are made from wires arranged linearly in a single direction or as a mesh. The corresponding detector active volume contains approximately 43 tonne of liquid xenon. Dual-phase xenon TPC technology will be employed as the baseline technology, in which the ionization signal is converted into proportional scintillation in the gaseous xenon between the gate and anode. Alternative options, for example, with proportional scintillation produced in liquid xenon [78, 79, 80] will also be explored. Since xenon procurement will likely take some time, the volume of the TPC needs to be easily upgraded based on the amount of xenon in possession. An acrylic barrel will be used as the major structural holder of the TPC. There is a very good assurance on the low radioactivity [81] since the acrylic panels used in JUNO have achieved a part-per-trillion (ppt) level of radio-impurity in mass production [82, 83]. The inner surface of the acrylic will be covered by a cylindrical sleeve of Polytetrafluoroethylene (PTFE) reflector of 2 mm-thickness to enhance the photon collection efficiency (VUV photon transmission for 2 mm PTFE is about 1% [84]). The field-shaping circuitry will be implemented on a cylindrical flexible printed circuit board sandwiched between the PTFE sleeve and acrylic barrel. The top and bottom of the TPC will be enclosed by two acrylic plates which contain holes to mount and support photosensors. Such a design is sufficiently robust and straightforward to be fabricated. Assuming that the photosensor arrays are constructed into the final form, the acrylic barrel structure will be the only component that gets swapped for each upgrade. One important design goal for PandaX-xT is to maximize the active volume. The volume of the 2-inch square-shape photosensors (see later) is significantly smaller than the 3-inch cylinder-shape ones used in previous generations of PandaX, LZ, and XENON. Such photosensor choice,

in combination with the low background acrylic fillers installed below the bottom array, will significantly reduce the dead volumes at the bottom of the detector. The xenon self-shielding areas in and around the TPC can be minimized given the reduction of material radioactivities and the IVETO/OVETO systems outside the inner vessel. With these measures, we target to control the dead volume to below 10% of total xenon (~ 47 tonne). The basic TPC performance parameters are: 1) a photon detection efficiency (g_1) of $>10\%$, 2) a drift field of >100 V/cm to allow for a 99.7% rejection of electron-recoil (ER) events, while maintaining a 50% efficiency on the DM-nuclear recoil (NR) events. These specifications have been mostly achieved in PandaX-II and PandaX-4T [49, 10]. The performance will be ensured through intensive calibrations, including the injection of radioisotopes to determine detector optical parameters, uniformity, and electron recoil (ER) responses [85, 86, 87, 88]. Additionally, various neutron sources, such as the deuteron-deuteron generator, will be used to obtain nuclear recoil (NR) responses [89, 90].

The photosensor arrays collect the 178 nm photons produced in the liquid and gaseous xenon, providing energy measurement as well as locations and sequences of energy depositions. The photosensitive area of PandaX-xT will exceed 10 m². In the past, significant saturation effects were observed in the Hamamatsu R11410 3-inch photomultiplier tubes (PMTs) in the MeV regime [37, 58, 91], limiting the energy linearity and resolution, and impairing the ability to reconstruct scattering positions in the LXe TPCs. Compared to R11410, Silicon Photomultipliers (SiPMs) have much better granularity and energy linearity, but unfortunately with relatively higher dark count rates under the LXe temperature (best-reported value 0.035-0.069 Hz/mm² [92], 3-7 times higher than that of R11410 [93]). The implementation of SiPM electronics would also be challenging due to the large number of channels. Therefore, a new type of photosensor with a square area of about 2.5×2.5 cm² per channel (Hamamatsu R12699) are being considered as the primary option for PandaX-xT, while we continue to closely monitor the technological advancements of SiPMs. In total, we expect a total of ~ 8000 independent channels if both top and bottom arrays are instrumented with R12699. Their fast (~ 1.2 ns) timing characteristics (vs. ~ 5.5 ns for R11410) will provide more information on the scintillation waveforms.

The readout electronics and data acquisition system digitizes the waveforms from photosensors and saves them on disk for future processing. They must support different data-taking rates in physics runs (~ 10 Hz) and calibration runs (>100 Hz). The readout system of PandaX-xT becomes much more challenging due to the large number of channels compared to PandaX-4T. The baseline solution involves using 500 MS/s 14-bit customized digitizers [94] which allows both single-channel-over-threshold readout or a firmware-based global readout trigger. Despite the maturity of the technology, it still needs to address the radioactivity and outgassing of thousands of mini-coaxial cables and the development of high-density low-temperature feedthroughs. As an alternative solution, cold electronics are under consideration for PandaX-xT. The system would be positioned near the photosensors inside the inner cryostat, digitize electrical signals and subsequently convert the data into optical signals using low-power transceivers. The system should feature high-speed sampling (> 100 MS/s) and low-power consumption (<100 mW/channel). Additionally, the front-end electronics should function fully at 178 K temperature and exhibit low radioactivity. The increasing sampling rate and expanding number of readout channels present significant challenges in data processing and storage. During the standard background data taking, assuming the sampling rate of 500 MS/s, it is estimated that over 5 TB of raw data will be generated per day. An upgrade of the data reduction strategy developed for PandaX-4T has the potential to effectively address these challenges [95].

The LXe handling system for the filling, recovery, and storage of xenon, dubbed First-X, allows xenon transfer in and out of the PandaX-xT detector entirely under the liquid form [96, 97]. This is imperative since the traditional filling and recuperation process with gaseous xenon becomes too time-consuming. The First-X system consists of multiple storage tanks, two cryogenic pumps, and the liquid nitrogen (LN2) and gas nitrogen (GN2) storage modules. Each storage tank is designed to store over 6 tonnes of xenon with an inner volume of 6.3 m³ and a design pressure of 7.1 MPa, satisfying the needs for long-term xenon storage in liquid phase (178 K, 0.2 MPa) or gaseous phase (300 K, 7.0 MPa). The storage tank's pressure can be rapidly regulated by three heat exchangers including two independent LN2-based cooling modules and one GN2-based heater. The cryogenic pump is a centrifugal pump with a magnetic drive that isolates the pump and LXe to avoid radioactivity contamination from the electric motor [98]. The First-X system with the initial six storage tanks has been constructed. The LXe filling/recovery mass flow rate has been demonstrated to reach 2.1 tonnes/hour.

The cryogenics and recirculation system provides cooling power for the LXe, while removing electronegative impurities with an active circulation loop and a purifier. The concept design is based on the successful operation of the cooling buses used in previous generations of PandaX [99, 100]. A preliminary estimate of the total heat load for PandaX-xT is about 1300 W at 178 K, including the radiation and conduction thermal loss of the IV (400 W), heat load of the gaseous circulation (100 W), and heat production by the frontend electronics (~ 800 W, if the option of cold electronics is adopted). A customized cooling tower with at least two GM Cryocoolers (Cryomech AL600, each with ~ 900 W cooling power at 178 K) will provide needed cooling power during regular operation. At the beginning of the experiment, an additional 2.5 kW of assistant cooling power [101] will be needed to cool down the LS as well as the IV

and OV to 178 K in 20 days. For this need, alternative means of cooling such as liquid nitrogen [102] will be incorporated via parallel cooling heads and loops. In addition, to achieve a long electron lifetime in the drifting field (>2 ms, corresponding to an electronegative impurity level of 10^{-10} mol/mol), a sufficiently fast recirculation speed is needed on both the liquid and gaseous xenon. The traditional gas recirculation with hot zirconium purifiers and heat exchangers can be used with a customized magnetically-coupled piston gas pump [103, 104]. A few such loops operating in parallel can achieve a 500 standard liters per minute (slpm) flow rate. Moreover, since O_2 is usually the dominant contributor to the attenuation of ionized electrons in liquid xenon, the liquid xenon recirculation (~ 2 lpm) with a cryogenic pump and O_2 sorbent will be used in parallel. This approach has been demonstrated to work very effectively in XENONnT [105, 106]. Special measures of radon control will be taken to avoid introducing radon into the TPC through the recirculation loops.

The distillation system removes the radioactive impurities such as ^{85}Kr , ^{222}Rn and tritium from the xenon. Krypton and radon are noble gas impurities originating either from external leaks or internal emanations, which cannot be removed by commercial purifiers. Tritium background was introduced in PandaX-II and PandaX-4T through tritiated-methane calibration injection, and the removal efficiency from the commercial purifier also appeared insufficient for a tritium level below 10^{-24} mol/mol [51, 10]. Cryogenic distillation is an effective technique to achieve ultra-pure xenon with a large flow rate based on the different boiling points of Xe, Kr, Rn, and tritiated methane (165 K, 120 K, 211 K and 111.5 K at atmospheric pressure, respectively), as demonstrated in earlier generations of PandaX [107, 108]. The requirements from PandaX-xT are more stringent (see Sec. 3), with levels of ^{85}Kr , ^{222}Rn and tritium lower than 2 nBq/kg, 0.5 $\mu\text{Bq/kg}$, and 0.01 nBq/kg, respectively. These are challenging specifications, and there have been a number of completed and ongoing developments by PandaX [96, 107, 108, 109, 110]. Quite some developments are also reported by XENON collaboration in this area [97, 111]. A new krypton-removal tower and radon-removal tower are under construction. According to the design, the krypton content in xenon could be reduced to 1×10^{-14} mol/mol (2 nBq/kg) at the flow rate of 30 kg/h with 99 % xenon collection efficiency. The krypton tower is expected to remove tritium in the xenon to a completely negligible level. For the radon tower, with a 5 lpm liquid xenon flow rate (860 kg/h), the radon reduction can reach a factor of 10 lower [110], achieving a level of 0.5 $\mu\text{Bq/kg}$ compared to 5 $\mu\text{Bq/kg}$ level in PandaX-4T without radon distillation [10]. These, together with other means of strict radioactivity control, are expected to lower the internal radioactive gas content to the desired values.

3 Background Estimation

The background level is the major driver of the scientific potential of PandaX-xT. For a multi-ten-tonne natural LXe detector, there are three major classes of background, 1) background arising from detector materials, 2) internal background from ^{85}Kr , ^{222}Rn , and tritium, and 3) physical background such as DBD events from ^{136}Xe and neutrino scattering events. The first component exhibits strong position dependence at the outskirts of the detector, so a proper fiducial volume selection can significantly reduce its contribution. The latter two components are uniformly distributed inside the detector. In this study, we assume that the background from the detector materials is primarily due to photosensor arrays and the copper vessel. The radioactivity levels are taken to be 0.02, 0.01 and 1.5 mBq/cm² for photosensors for ^{238}U , ^{232}Th , and ^{40}K , respectively, based on prototype sample measurements, and 5 ppt of ^{238}U , ^{232}Th , and ^{40}K for the copper vessel (achieved in Majorana Demonstrator, EXO-200, and SuperCDMS experiments [112, 113, 114]). The radioactivity of PTFE in the TPC is assumed to be 1 ppt for ^{238}U and 10 ppt for ^{232}Th , producing a negligible background. For the internal background in LXe, we assume a level of 2 nBq/kg and 0.5 $\mu\text{Bq/kg}$ for ^{85}Kr and ^{222}Rn , respectively. For the physical background, the rates and energy spectra are taken from Ref. [13], except those for the double electron-capture of ^{124}Xe , which are taken from the recent measurement from XENONnT [115]. The cosmogenically produced ^{137}Xe is assumed to be two orders of magnitude less in comparison to that estimated in DARWIN [116], scaled using the total muon rate ratio between the CJPL and LNGS [117].

A customized Geant4 simulation, BambooMC [118], is used to estimate the background in PandaX-xT using a simplified geometry in Fig. 2. The approach is very similar to that for Pandax-4T [44, 60]. The intrinsic decay class in Geant4 is used to simulate radioactive decay chains, with all energy depositions inside the detector and veto detectors recorded, allowing a straightforward evaluation of the ER background. The neutron production arising from material radioactivities is simulated using a neutron generator improved from the traditional SOURCES-4A [119], which utilizes an updated nuclear cascade model and fission model implemented in Geant4 to properly take into account correlated emissions of neutron and gamma ray(s) as well as multiple neutrons [120, 118].

Four sets of cuts are developed in simulation to select candidates, namely the single-scatter cut, veto cuts, energy region of interest (ROI) cuts, and fiducial volume (FV) cuts:

1. Single-scatter cut rejects events with multiple energy depositions in the detector simulation.
2. Veto cuts remove events with energy deposition greater than 200 keV in the IVETO region. While the

OVETO will operate at the same time providing additional veto efficiency, we omit its contribution in this study for conservativeness.

- ROI cuts are defined for three main physics regions. The DM ROI, [1, 10] keV_{ee}, includes both low energy ER and NR background (neutron and neutrino-nuclear coherent scattering) events. The solar neutrino ROI, [10, 150] keV_{ee}, refers to the primary energy region for elastic-electron scattering signals from solar *pp* neutrinos [121]. The NLDBD ROI, [2433, 2483] keV_{ee}, covers a 50-keV window around the *Q*-value of ¹³⁶Xe NLDBD (2458 keV). To implement a simplified energy response model, the ER energy deposition is smeared with a resolution function σ/E of $30\%/\sqrt{E/\text{keV}} + 0.4\%$. The NR energy is converted into an equivalent ER energy using the Lindhard factor [122, 123] but without the smearing.
- FV cuts are optimized with a simple “cut-and-count” figure-of-merit $\frac{\epsilon M \times T}{\sqrt{B}}$ in which ϵ is the signal efficiency, M is the fiducial mass, T is the data taking time, and B is the corresponding number of background events. For the DM ROI, since the signal is the DM-nucleus NR scattering, we assume an ER background rejection power of 99.7% and an NR acceptance of 50% with the standard ionization-to-scintillation ratio cut in LXe DM experiments. There is only ER background in the solar neutrino and NLDBD ROIs. The resulting optimized cylindrical FV for the DM and solar neutrino region is 34.2 tonne (190 mm to the top, 170 mm to the bottom, and 102 mm to the side of the TPC) and NLDBD is 8.4 tonne (780 mm to the top, 816 mm to the bottom, and 484 mm to the side of the TPC) of natural xenon.

After these cuts, background energy spectra below 150 keV (the DM and solar neutrino-electron scattering regions) and the high energy NLDBD region are shown in Figs. 3 and 4. Corresponding background events in the DM, solar neutrino, and NLDBD energy regions are summarized in Tables 1, 2, and 3. Note that the background rate in the NLDBD ROI is highly sensitive to the background assumption, so the results of a “baseline” and “ideal” assumption are given. Under the “baseline” assumption, one major background arises from the ²¹⁴Bi β -decay, the daughters of the internal ²²²Rn daughter. Although ²¹⁴Bi can be very efficiently tagged and vetoed via the delayed coincidence of ²¹⁴Bi–²¹⁴Po decay, we assume a 0.1% residual untagged ²¹⁴Bi nevertheless. Under the “ideal” assumption, we assume that the material background is reduced by 5 times from the “baseline” and the background from ²²²Rn is negligible.

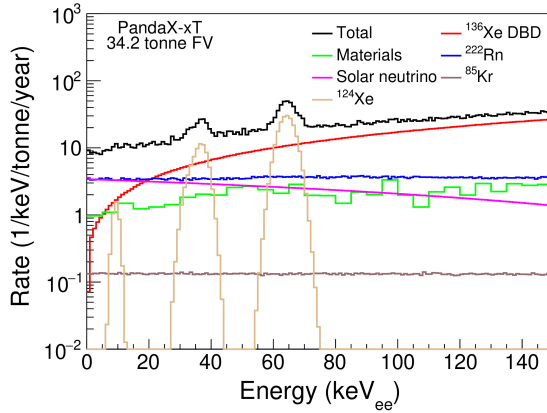


Figure 3: The energy spectra of individual background components between 1 and 150 keV (DM and solar neutrino regions) with SS, veto, and FV cuts applied.

4 Physics potential

Being an unique deep underground and ultralow background liquid xenon observatory, the physics potential of PandaX-xT is very rich. Instead of presenting an exhaustive list of physics [125], we benchmark the capability of PandaX-xT in the WIMP search, NLDBD, and solar neutrino detection, covering an effective energy range from keV to MeV. Within these energy windows, the sensitivity of alternative signals with a single-scattering nature can be estimated based on the background rate presented in the previous section. The sensitivities to more exotic signals, for example, with multiple energy depositions via nuclear or atomic excitations or with time correlations, have to be studied case by case and are beyond the scope of this paper.

For the WIMP search in the DM ROI, the background level is 75 events/tonne/year for electron recoil (ER) and 0.02 events/tonne/year for NR, respectively (Table 1). With the simple “cut-and-count” assumptions of an ER background rejection power of 99.7% and an NR acceptance of 50%, the ER and

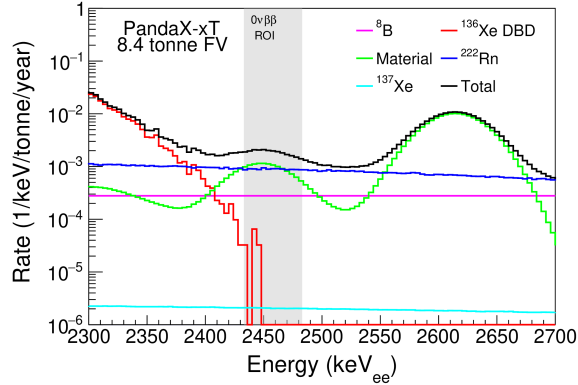


Figure 4: The energy spectra of individual background components in the MeV region with SS, veto, and FV cuts applied under the “baseline” background assumption. See text for details.

Table 1: Expected background for the DM search region between 1 to 10 keV_{ee}. The FV mass is 34.2 tonnes. The rates are obtained without applying the ER/NR rejection cut.

	ER (event/tonne/year)	NR (event/tonne/year)
Photosensors	8.3	0.00007
Copper vessel	0.02	0.000002
⁸⁵ Kr	1.2	-
²²² Rn	28.2	-
¹³⁶ Xe	9.6	-
Solar ν	27.5	-
Atmospheric ν	0.0	0.02
Diffusive supernova ν	0.0	0.002
Total	74.8	0.02

NR backgrounds in the ROI are 0.23 events/tonne/year and 0.01 events/tonne/year, respectively. Note that the accidental background has been omitted in the WIMP ROI to be consistent with the assumptions in previous studies, e.g. by DARWIN [126], and they are sub-dominant in the current generation experiments. With the standard DM halo and nuclear form factors parameters, and the spin-independent or spin-dependent isospin-conserving DM-nucleon interaction [127], and with a projected exposure of 200 tonne-year, the sensitivities are summarized in Fig. 5. Note that the PandaX-xT sensitivity reached about $3.5 \times 10^{-49} \text{ cm}^2$ for spin-independent interactions at a DM mass of 40 GeV/ c^2 . The sensitivity is expected to improve with a likelihood approach with the full distributions of the signal and background incorporated. Nevertheless, the limit covers most of the allowed parameter space from the constrained minimal Supersymmetry models [128]. Also overlaid is the neutrino-background-only sensitivity “floor” with three neutrino-nucleus coherent scattering events from Ref. [13]. The sensitivities to the spin-dependent interactions with the proton and neutron are also given in the figure.

Table 2: Expected background for the solar neutrino-electron elastic scattering region between 10 to 150 keV for the 34.2-tonne FV. For comparison, the solar neutrino signal is calculated based on the Standard Solar Model [124].

	ER (event/tonne/year)
Photosensors	270
Copper vessel	21
⁸⁵ Kr	19
²²² Rn	439
¹³⁶ Xe	1927
¹²⁴ Xe	276
Solar ν	343

Table 3: Expected background under the baseline and ideal scenarios for the NLDBD energy range between 2433 and 2483 keV for the 8.4-tonne FV. See text for details.

	Baseline (event/tonne/year)	Ideal (event/tonne/year)
Photosensors	1.4×10^{-2}	2.8×10^{-3}
Copper vessel	2.9×10^{-2}	5.8×10^{-3}
^{222}Rn	4.5×10^{-2}	-
^{136}Xe DBD	5.2×10^{-4}	5.2×10^{-4}
^{137}Xe	1.0×10^{-4}	1.0×10^{-4}
Solar ^8B ν	1.4×10^{-2}	1.4×10^{-2}
Total	1.1×10^{-1}	2.4×10^{-2}

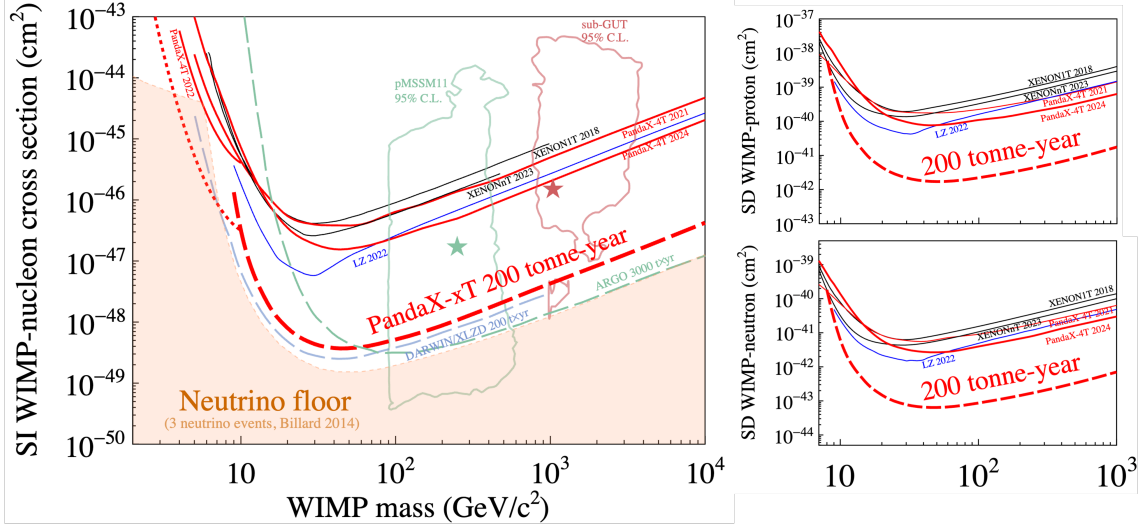


Figure 5: Projected 90% C.L. exclusion sensitivities (red dashed curve) of PandaX-xT to spin-independent, and spin-dependent WIMP-neutron/-proton interactions estimated with a cut-and-count method, assuming the background level from Table 1, a 99.7% ER rejection power and a 50% NR acceptance, and an exposure of 200 tonne-year. Our benchmark energy range from 1 to 10 keV_{ee} has limited our sensitivity to DM masses less than 10 GeV/c². The sensitivity curve for low-mass DM below 10 GeV/c² (dotted line in the left graph) is estimated based on the PandaX-4T efficiency curve in a specialized low energy analysis in Ref. [129], and a 1:1 ratio of ^8B neutrino induced CE ν NS and accidental coincidence background. The “neutrino floor” (3 events) and 95% C.L. contour of allowed parameter space in Supersymmetry models are taken from Refs. [13] and [128], respectively. Past experimental constraints [10, 50, 49, 130, 131, 53, 132, 133, 11, 12] are also overlaid. We also overlay sensitivities of the future DARWIN/XLZD [134] and ARGO [135] with exposure indicated.

For NLDBD, at the Q -value of ^{136}Xe NLDBD (2458 keV), and with an energy resolution σ/E of 1%, the level of the background for the 8.4-tonne fiducial volume is 2.1×10^{-3} count/keV/tonne/year within a 50 keV energy window (Table 3). The sensitivity to the NLDBD half-life can be expressed as

$$T_{1/2}^{\text{NLDBD}} = \frac{\ln 2 \times \epsilon \times f_{\text{ROI}} \times (\# \text{ of } ^{136}\text{Xe atoms}) \times T}{1.64\sqrt{B}}, \quad (1)$$

in which $f_{\text{ROI}} = 0.68$ is the fraction of events enclosed in the NLDBD ROI, ϵ is the signal selection efficiency which is assumed to be 100%, B is the number of background events (Table 3), the number of ^{136}Xe atoms is calculated assuming natural abundance, and $T = 10$ years. This leads to a half-life sensitivity of 3.3×10^{27} and 6.9×10^{27} years for the baseline and ideal background assumptions, respectively. The baseline result corresponds to an upper limit of the effective Majorana mass between [10 – 41] meV/c² on $m_{\beta\beta}$, in which the spread is due to the uncertainty in the nuclear matrix elements [136]. The sensitivity can mostly cover the allowed space for inverted neutrino MO, assuming that NLDBD is mediated by light Majorana neutrinos, as illustrated in Fig. 6.

For the solar neutrinos, we benchmark our sensitivity to the solar ^8B neutrino flux via coherent elastic neutrino-nucleus scattering (CE ν NS), and the pp neutrino flux via neutrino-electron elastic scattering. With 200 tonne-year exposure, the number of detected ^8B neutrino CE ν NS events is approximately 710, conservatively estimated based on the PandaX-4T efficiency curve in a specialized low energy analysis in Ref. [129], with an energy threshold of ~ 0.95 keV_{nr} (1% efficiency) and the energy smearing taken into

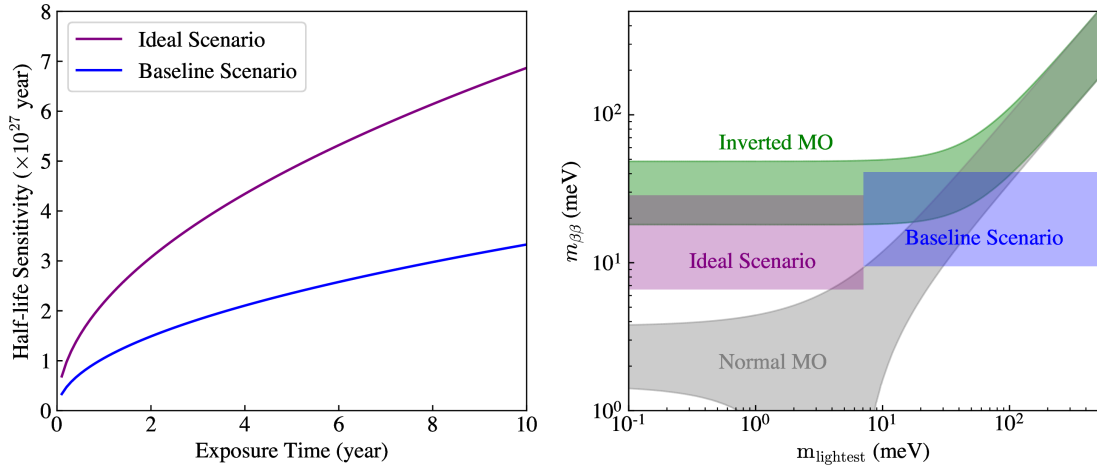


Figure 6: (Left) Projected 90% C.L. sensitivity to NLDBD half-life as a function of exposure time for the baseline and ideal background scenarios, assuming a fiducial mass of 8.4-ton natural xenon. Inputs used in the calculation are in Table 3 and discussed in the text. (Right) Effective Majorana mass ($m_{\beta\beta}$) sensitivity with 10 year of exposure with respect to the phase space of the inverted and normal MO of neutrinos. The sensitivity bands of the two scenarios are due to the spread of commonly-used nuclear matrix elements. The two sensitivity bands are staggered intentionally for better visibility.

account. With an additional assumption of an equal number of accidental background events, PandaX-xT is capable of making a better-than 10% precision measurement on the ^8B neutrino fluxes (Fig. 7). We expect the efficiency and accidental background to be further improved along the way. For the pp neutrinos, assuming a 2% systematic uncertainty for material, krypton and radon background, the relative precision of pp flux can be determined to 3% using ER spectra fitting, better than the current best measurement from Borexino [137].

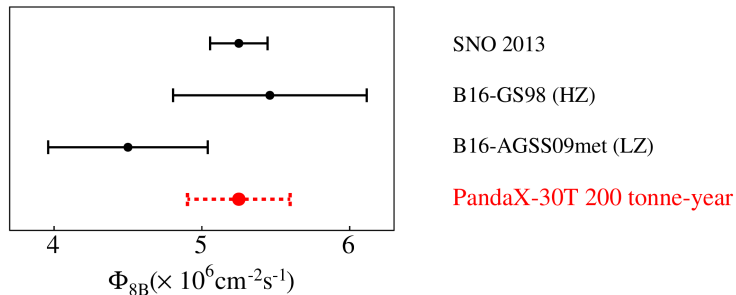


Figure 7: Projected sensitivity of PandaX-xT to solar ^8B neutrino flux assuming the same mean value as SNO [138], compared with theoretical models [139].

Note that the neutrino scattering rate in Tables 1 and 2 has assumed standard electroweak interaction only. If there is an enhanced neutrino magnetic moment μ_ν due to the Majorana nature or exotic new physics beyond the SM, the elastic scattering cross section will be modified by a term [13]

$$\left(\frac{d\sigma}{dT}\right)_{\mu_\nu} = \frac{\pi\alpha_{\text{EM}}^2\mu_\nu^2}{m_e^2} \left[\frac{1-T/E_\nu}{T}\right], \quad (2)$$

in which $\alpha_{\text{EM}} = 1/137$, m_e is the mass of the electron, and E_ν and T are the energy of the neutrino and recoiled electron, respectively. Therefore, the low energy pp neutrino measurement can be in turn used to search for μ_ν . With 200 tonne-year exposure and our background presented in the ROI of DM in Table 1, we expect to achieve an unprecedented sensitivity of $1.2 \times 10^{-12} \mu_B$ to μ_ν (Fig. 8), where μ_B is the Bohr magneton.

5 Discussions and Conclusions

This paper is a combination of letter-of-intent of PandaX-xT, a concise description of major design concepts, and physics potentials if the assumed performances are met. One should note that some of the technical choices presented still require significant R&D. In Table 4, we summarize the readiness of individual subsystems and key techniques.

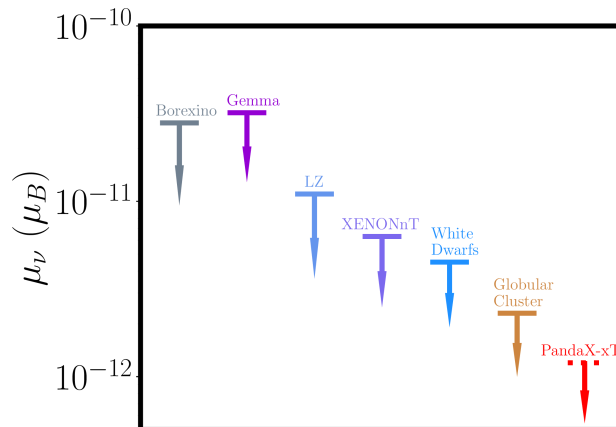


Figure 8: The sensitivity on the neutrino magnetic moment (90% C.L.) of PandaX-xT with 200 tonne-year exposure (red), together with constraints from current leading experiments [140, 105, 141, 142] and astrophysical observations [143, 144].

Table 4: Project requirements and challenges. The \star , $\star\star$, and $\star\star\star$ represent existing technology, what requires some R&D but relies on well-established principles, and what is R&D with uncertain outcome, respectively.

Item	Design goal	Current status	Challenge level
Low background cryostat	thin-walled Cu	Low background SS	$\star\star\star$
LXe TPC	2.6 m (\varnothing) \times 3.0 m (H)	1.2 m (\varnothing) \times 1.2 m (H)	$\star\star$
Photosensor array	10 m ² , high QE, low noises, fast	3 m ² , R11410 3" PMT	\star
Readout electronics	Cold and low background	Custom digitizer, outside, 500 MS/s	$\star\star\star$
Energy resolution at 2.5 MeV	1%	1.9%	\star
⁸⁵ Kr background	2 nBq/kg	60 nBq/kg	$\star\star$
²²² Rn background	0.5 μ Bq/kg	5 μ Bq/kg	$\star\star$
Cryogenics & recirculation	500 slpm gas (2 lpm liquid)	150 slpm gas	$\star\star$
IVETO	200 keV threshold	under R&D	$\star\star\star$

Besides the standard methods of background rejection through data selection cuts, new methods are also being pursued by the PandaX collaboration. We anticipate improved measurement of the scintillation timing profiles for different recoil events [145, 146, 147] by utilizing the fast time response of the R12699. In the spatial dimension, we plan to reconstruct individual scattering vertices to a sub-centimeter resolution, and track features in β s will be explored, to reduce the background in the MeV energy region. Taking further advantage of the photosensors with \sim ns timing response, we plan to investigate the detection of Cherenkov photons using both temporal and spatial information, a new method for background discrimination in the MeV region [148].

CJPL is being transformed into a mature national facility [52], and most of the infrastructure from PandaX-4T will be inherited. These will ease the deployment of PandaX-xT. The CJPL site provides additional key advantages to PandaX-xT. The large overburden gives a much lower cosmogenic background in comparison to laboratories at shallower sites, in particular ¹³⁷Xe. The low latitude (28°N) of CJPL and the higher field strength parallel to the earth’s surface thereby suppresses low energy cosmic rays entering the atmosphere. This leads to a more than two times lower atmospheric neutrino background, the “ultimate” background for DM direct detection in the high mass region (>10 GeV/ c^2), than those of high-latitude underground laboratories (LNGS, SURF, and SNOLAB) [149, 70]. Note that the prediction of the atmospheric neutrino flux and spectrum has rather large uncertainty. The PandaX-xT OVETO could enable a measurement of atmospheric neutrino flux at CJPL.

PandaX-xT is envisioned to be carried out in multiple phases. In the first phase, natural xenon will be used as the detection target. We will gradually upgrade the detector based on the xenon in possession, reach a total target mass of 43 tonnes and operate for more than 10 years. In the next phase, we envision that isotopic separation technology will be used to produce xenon with artificially modified isotopic abundance (AMIA), either via a split of odd and even nuclei [150], or further enrichment of ¹³⁶Xe. Two functionally identical detectors can be filled with different AMIA xenon and operated simultaneously. Two identical detectors but with different nuclear spins allows one to explore the SI and SD nature of the DM interactions. The sensitivity to NLDBD can also be greatly improved by this “dual-detector mode”.

To summarize, we have demonstrated that the proposed PandaX-xT detector, with a 43 tonne active xenon target, will be a cutting-edge and multi-purpose observatory covering a wide range of physics topics in particle physics and astrophysics. With an exposure of 200 tonne-year, it allows a search sensitivity for DM-nucleon interactions to the neutrino floor [13, 14, 151], a key test on the WIMP DM. The same

detector, operated for 10 years, will provide stringent tests on the Majorana nature of neutrinos using the NLDBD of ^{136}Xe , effectively covering most of the parameter space for inverted neutrino MO. With its uniqueness in detecting low energy recoils, PandaX-xT will also allow precise detection of solar ^8B and pp neutrinos, as well as other neutrinos with astrophysical origins. These neutrinos can be used to broadly search for new physics, as well as in the context of multi-messenger astronomy, such as detecting supernova explosions.

6 Acknowledgement

This project is supported in part by the Office of Science and Technology, Shanghai Municipal Government (grant Nos. 23JC1410200 and 22JCJC1410200), the Ministry of Science and Technology of China (grant No. 2023YFA1606200), and the National Science Foundation of China (grant Nos. 1209060, 12005131, 11905128, 11925502, 12222505, 12175139). We thank support from Double First Class Plan of the Shanghai Jiao Tong University, and the Tsung-Dao Lee Institute Experimental Platform Development Fund. We also thank the sponsorship from the Hongwen Foundation in Hong Kong, Tencent and New Cornerstone Science Foundation in China, and Yangyang Development Fund. Finally, we thank the CJPL administration and the Yalong River Hydropower Development Company Ltd. for indispensable logistical support and other help.

References

- [1] G. Bertone, D. Hooper, J. Silk, Particle dark matter: Evidence, candidates and constraints, *Phys. Rept.* 405 (2005) 279–390. [arXiv:hep-ph/0404175](#), [doi:10.1016/j.physrep.2004.08.031](#).
- [2] G. Jungman, M. Kamionkowski, K. Griest, Supersymmetric dark matter, *Phys. Rept.* 267 (1996) 195–373. [arXiv:hep-ph/9506380](#), [doi:10.1016/0370-1573\(95\)00058-5](#).
- [3] M. W. Goodman, E. Witten, Detectability of Certain Dark Matter Candidates, *Phys. Rev. D* 31 (1985) 3059. [doi:10.1103/PhysRevD.31.3059](#).
- [4] R. J. Gaitskell, Direct detection of dark matter, *Ann. Rev. Nucl. Part. Sci.* 54 (2004) 315–359. [doi:10.1146/annurev.nucl.54.070103.181244](#).
- [5] T. Marrodán Undagoitia, L. Rauch, Dark matter direct-detection experiments, *J. Phys. G* 43 (1) (2016) 013001. [arXiv:1509.08767](#), [doi:10.1088/0954-3889/43/1/013001](#).
- [6] J. Liu, X. Chen, X. Ji, Current status of direct dark matter detection experiments, *Nature Phys.* 13 (3) (2017) 212–216. [arXiv:1709.00688](#), [doi:10.1038/nphys4039](#).
- [7] M. Schumann, Direct Detection of WIMP Dark Matter: Concepts and Status, *J. Phys. G* 46 (10) (2019) 103003. [arXiv:1903.03026](#), [doi:10.1088/1361-6471/ab2ea5](#).
- [8] J. Billard, et al., Direct detection of dark matter—APPEC committee report, *Rept. Prog. Phys.* 85 (5) (2022) 056201. [arXiv:2104.07634](#), [doi:10.1088/1361-6633/ac5754](#).
- [9] P. Cushman, et al., Working Group Report: WIMP Dark Matter Direct Detection, in: *Snowmass 2013: Snowmass on the Mississippi*, 2013. [arXiv:1310.8327](#).
- [10] Y. Meng, et al., Dark Matter Search Results from the PandaX-4T Commissioning Run, *Phys. Rev. Lett.* 127 (26) (2021) 261802. [arXiv:2107.13438](#), [doi:10.1103/PhysRevLett.127.261802](#).
- [11] E. Aprile, et al., First Dark Matter Search with Nuclear Recoils from the XENONnT Experiment, *Phys. Rev. Lett.* 131 (4) (2023) 041003. [arXiv:2303.14729](#), [doi:10.1103/PhysRevLett.131.041003](#).
- [12] J. Aalbers, et al., First Dark Matter Search Results from the LUX-ZEPLIN (LZ) Experiment, *Phys. Rev. Lett.* 131 (4) (2023) 041002. [arXiv:2207.03764](#), [doi:10.1103/PhysRevLett.131.041002](#).
- [13] J. Billard, L. Strigari, E. Figueroa-Feliciano, Implication of neutrino backgrounds on the reach of next generation dark matter direct detection experiments, *Phys. Rev. D* 89 (2) (2014) 023524. [arXiv:1307.5458](#), [doi:10.1103/PhysRevD.89.023524](#).
- [14] C. A. J. O’Hare, New Definition of the Neutrino Floor for Direct Dark Matter Searches, *Phys. Rev. Lett.* 127 (25) (2021) 251802. [arXiv:2109.03116](#), [doi:10.1103/PhysRevLett.127.251802](#).
- [15] E. Majorana, Teoria simmetrica dell’elettrone e del positrone, *Nuovo Cim.* 14 (1937) 171–184. [doi:10.1007/BF02961314](#).
- [16] P. Minkowski, $\mu \rightarrow e\gamma$ at a Rate of One Out of 10^9 Muon Decays?, *Phys. Lett. B* 67 (1977) 421–428. [doi:10.1016/0370-2693\(77\)90435-X](#).
- [17] T. Yanagida, Proc. workshop on unified theory and the baryon number in the universe, KEK Report No. 79-18 95 (1979).
- [18] M. Gell-Mann, P. Ramond, R. Slansky, Complex Spinors and Unified Theories, *Conf. Proc. C* 790927 (1979) 315–321. [arXiv:1306.4669](#).
- [19] S. L. Glashow, The Future of Elementary Particle Physics, *NATO Sci. Ser. B* 61 (1980) 687. [doi:10.1007/978-1-4684-7197-7_15](#).
- [20] R. N. Mohapatra, G. Senjanovic, Neutrino Mass and Spontaneous Parity Nonconservation, *Phys. Rev. Lett.* 44 (1980) 912. [doi:10.1103/PhysRevLett.44.912](#).
- [21] M. Fukugita, T. Yanagida, Baryogenesis Without Grand Unification, *Phys. Lett. B* 174 (1986) 45–47. [doi:10.1016/0370-2693\(86\)91126-3](#).
- [22] W. H. Furry, On transition probabilities in double beta-disintegration, *Phys. Rev.* 56 (1939) 1184–1193. [doi:10.1103/PhysRev.56.1184](#).
- [23] M. Agostini, G. Benato, J. A. Detwiler, J. Menéndez, F. Vissani, Toward the discovery of matter creation with neutrinoless $\beta\beta$ decay, *Rev. Mod. Phys.* 95 (2) (2023) 025002. [arXiv:2202.01787](#), [doi:10.1103/RevModPhys.95.025002](#).
- [24] M. Agostini, et al., Final Results of GERDA on the Search for Neutrinoless Double- β Decay, *Phys. Rev. Lett.* 125 (25) (2020) 252502. [arXiv:2009.06079](#), [doi:10.1103/PhysRevLett.125.252502](#).
- [25] I. J. Arnquist, et al., Final Result of the Majorana Demonstrator’s Search for Neutrinoless Double- β Decay in Ge76, *Phys. Rev. Lett.* 130 (6) (2023) 062501. [arXiv:2207.07638](#), [doi:10.1103/PhysRevLett.130.062501](#).

- [26] G. Anton, et al., Search for Neutrinoless Double- β Decay with the Complete EXO-200 Dataset, *Phys. Rev. Lett.* 123 (16) (2019) 161802. [arXiv:1906.02723](#), [doi:10.1103/PhysRevLett.123.161802](#).
- [27] D. Q. Adams, et al., Search for Majorana neutrinos exploiting millikelvin cryogenics with CUORE, *Nature* 604 (7904) (2022) 53–58. [arXiv:2104.06906](#), [doi:10.1038/s41586-022-04497-4](#).
- [28] V. Albanese, et al., The SNO+ experiment, *JINST* 16 (08) (2021) P08059. [arXiv:2104.11687](#), [doi:10.1088/1748-0221/16/08/P08059](#).
- [29] R. Arnold, et al., Results of the search for neutrinoless double- β decay in ^{100}Mo with the NEMO-3 experiment, *Phys. Rev. D* 92 (7) (2015) 072011. [arXiv:1506.05825](#), [doi:10.1103/PhysRevD.92.072011](#).
- [30] S. Abe, et al., Search for the Majorana Nature of Neutrinos in the Inverted Mass Ordering Region with KamLAND-Zen, *Phys. Rev. Lett.* 130 (5) (2023) 051801. [arXiv:2203.02139](#), [doi:10.1103/PhysRevLett.130.051801](#).
- [31] G. Adhikari, et al., nEXO: neutrinoless double beta decay search beyond 10^{28} year half-life sensitivity, *J. Phys. G* 49 (1) (2022) 015104. [arXiv:2106.16243](#), [doi:10.1088/1361-6471/ac3631](#).
- [32] R. Nakamura, H. Sambonsugi, K. Shiraishi, Y. Wada, Research and development toward KamLAND2-Zen, *J. Phys. Conf. Ser.* 1468 (1) (2020) 012256. [doi:10.1088/1742-6596/1468/1/012256](#).
- [33] R. Brugnera, Neutrinoless double beta decay search with LEGEND, *PoS NOW2022* (2023) 075. [doi:10.22323/1.421.0075](#).
- [34] H. Ma, W. Dai, L. Yang, CDEX-300 ν program for Ge-76 neutrinoless double beta decay search, *PoS TAUP2023* (2024) 200. [doi:10.22323/1.441.0200](#).
- [35] J. Zhao, L.-J. Wen, Y.-F. Wang, J. Cao, Physics potential of searching for $0\nu\beta\beta$ decays in JUNO, *Chin. Phys. C* 41 (5) (2017) 053001. [arXiv:1610.07143](#), [doi:10.1088/1674-1137/41/5/053001](#).
- [36] K. Alfonso, et al., CUPID: The Next-Generation Neutrinoless Double Beta Decay Experiment, *J. Low Temp. Phys.* 211 (5-6) (2023) 375–383. [doi:10.1007/s10909-022-02909-3](#).
- [37] E. Aprile, et al., Energy resolution and linearity of XENON1T in the MeV energy range, *Eur. Phys. J. C* 80 (8) (2020) 785. [arXiv:2003.03825](#), [doi:10.1140/epjc/s10052-020-8284-0](#).
- [38] G. Pereira, C. Silva, V. N. Solovov, Energy resolution of the LZ detector for high-energy electronic recoils, *JINST* 18 (04) (2023) C04007. [doi:10.1088/1748-0221/18/04/C04007](#).
- [39] J. Aalbers, et al., A next-generation liquid xenon observatory for dark matter and neutrino physics, *J. Phys. G* 50 (1) (2023) 013001. [arXiv:2203.02309](#), [doi:10.1088/1361-6471/ac841a](#).
- [40] J. Aalbers, et al., DARWIN: towards the ultimate dark matter detector, *JCAP* 11 (2016) 017. [arXiv:1606.07001](#), [doi:10.1088/1475-7516/2016/11/017](#).
- [41] **XLZD: Joining forces towards a next-generation Dark Matter experiment**, <https://darwin.physik.uzh.ch/news.html>, <https://xlzd.org>.
URL <https://darwin.physik.uzh.ch/news.html>, <https://xlzd.org>
- [42] J.-P. Cheng, et al., The China Jinping Underground Laboratory and its Early Science, *Ann. Rev. Nucl. Part. Sci.* 67 (2017) 231–251. [arXiv:1801.00587](#), [doi:10.1146/annurev-nucl-102115-044842](#).
- [43] X. Cao, et al., PandaX: A Liquid Xenon Dark Matter Experiment at CJPL, *Sci. China Phys. Mech. Astron.* 57 (2014) 1476–1494. [arXiv:1405.2882](#), [doi:10.1007/s11433-014-5521-2](#).
- [44] H. Zhang, et al., Dark matter direct search sensitivity of the PandaX-4T experiment, *Sci. China Phys. Mech. Astron.* 62 (3) (2019) 31011. [arXiv:1806.02229](#), [doi:10.1007/s11433-018-9259-0](#).
- [45] K.-J. Kang, et al., Introduction to the CDEX experiment, *Front. Phys. (Beijing)* 8 (2013) 412–437. [arXiv:1303.0601](#), [doi:10.1007/s11467-013-0349-1](#).
- [46] Q. Yue, et al., Limits on light WIMPs from the CDEX-1 experiment with a p-type point-contact germanium detector at the China Jinping Underground Laboratory, *Phys. Rev. D* 90 (2014) 091701. [arXiv:1404.4946](#), [doi:10.1103/PhysRevD.90.091701](#).
- [47] H. Jiang, et al., Limits on Light Weakly Interacting Massive Particles from the First 102.8 kg \times day Data of the CDEX-10 Experiment, *Phys. Rev. Lett.* 120 (24) (2018) 241301. [arXiv:1802.09016](#), [doi:10.1103/PhysRevLett.120.241301](#).
- [48] M. Xiao, et al., First dark matter search results from the PandaX-I experiment, *Sci. China Phys. Mech. Astron.* 57 (2014) 2024–2030. [arXiv:1408.5114](#), [doi:10.1007/s11433-014-5598-7](#).
- [49] A. Tan, et al., Dark Matter Results from First 98.7 Days of Data from the PandaX-II Experiment, *Phys. Rev. Lett.* 117 (12) (2016) 121303. [arXiv:1607.07400](#), [doi:10.1103/PhysRevLett.117.121303](#).

- [50] X. Cui, et al., Dark Matter Results From 54-Ton-Day Exposure of PandaX-II Experiment, *Phys. Rev. Lett.* 119 (18) (2017) 181302. [arXiv:1708.06917](#), [doi:10.1103/PhysRevLett.119.181302](#).
- [51] X. Zhou, et al., A Search for Solar Axions and Anomalous Neutrino Magnetic Moment with the Complete PandaX-II Data, *Chin. Phys. Lett.* 38 (1) (2021) 011301. [arXiv:2008.06485](#), [doi:10.1088/0256-307X/38/10/109902](#).
- [52] J. Li, X. Ji, W. Haxton, J. S. Y. Wang, The second-phase development of the China JinPing underground Laboratory, *Phys. Procedia* 61 (2015) 576–585. [doi:10.1016/j.phpro.2014.12.055](#).
- [53] Z. Huang, et al., Constraints on the axial-vector and pseudo-scalar mediated WIMP-nucleus interactions from PandaX-4T experiment, *Phys. Lett. B* 834 (2022) 137487. [arXiv:2208.03626](#), [doi:10.1016/j.physletb.2022.137487](#).
- [54] S. Li, et al., Search for Light Dark Matter with Ionization Signals in the PandaX-4T Experiment, *Phys. Rev. Lett.* 130 (26) (2023) 261001. [arXiv:2212.10067](#), [doi:10.1103/PhysRevLett.130.261001](#).
- [55] D. Huang, et al., Search for Dark-Matter–Nucleon Interactions with a Dark Mediator in PandaX-4T, *Phys. Rev. Lett.* 131 (19) (2023) 191002. [arXiv:2308.01540](#), [doi:10.1103/PhysRevLett.131.191002](#).
- [56] X. Ning, et al., Limits on the luminance of dark matter from xenon recoil data, *Nature* 618 (7963) (2023) 47–50. [doi:10.1038/s41586-023-05982-0](#).
- [57] Y. Bai, Dark Matter is Darker, *NUCLEAR SCIENCE AND TECHNIQUES* 34 (6) (2023) 76. [doi:10.1007/s41365-023-01249-5](#).
- [58] L. Si, et al., Determination of Double Beta Decay Half-Life of ^{136}Xe with the PandaX-4T Natural Xenon Detector, *Research* 2022 (2022) 9798721. [arXiv:2205.12809](#), [doi:10.34133/2022/9798721](#).
- [59] X. Yan, et al., Searching for Two-Neutrino and Neutrinoless Double Beta Decay of Xe^{134} with the PandaX-4T Experiment, *Phys. Rev. Lett.* 132 (15) (2024) 152502. [arXiv:2312.15632](#), [doi:10.1103/PhysRevLett.132.152502](#).
- [60] Z. Qian, et al., Low radioactive material screening and background control for the PandaX-4T experiment, *JHEP* 06 (2022) 147. [arXiv:2112.02892](#), [doi:10.1007/JHEP06\(2022\)147](#).
- [61] H. Ma, W. Dai, Z. Zeng, T. Xue, L. Yang, Q. Yue, J. Cheng, *Status and prospect of china jinping underground laboratory*, *Journal of Physics: Conference Series* 2156 (1) (2021) 012170. [doi:10.1088/1742-6596/2156/1/012170](#).
URL <https://dx.doi.org/10.1088/1742-6596/2156/1/012170>
- [62] S. Agostinelli, et al., GEANT4—a simulation toolkit, *Nucl. Instrum. Meth. A* 506 (2003) 250–303. [doi:10.1016/S0168-9002\(03\)01368-8](#).
- [63] M. Yeh, S. Hans, W. Beriguete, R. Rosero, L. Hu, R. L. Hahn, M. V. Diwan, D. E. Jaffe, S. H. Kettell, L. Littenberg, A new water-based liquid scintillator and potential applications, *Nucl. Instrum. Meth. A* 660 (2011) 51–56. [doi:10.1016/j.nima.2011.08.040](#).
- [64] J. R. Alonso, et al., Advanced Scintillator Detector Concept (ASDC): A Concept Paper on the Physics Potential of Water-Based Liquid Scintillator (9 2014). [arXiv:1409.5864](#).
- [65] L. J. Bignell, et al., Characterization and Modeling of a Water-based Liquid Scintillator, *JINST* 10 (12) (2015) P12009. [arXiv:1508.07029](#), [doi:10.1088/1748-0221/10/12/P12009](#).
- [66] M. Askins, et al., THEIA: an advanced optical neutrino detector, *Eur. Phys. J. C* 80 (5) (2020) 416. [arXiv:1911.03501](#), [doi:10.1140/epjc/s10052-020-7977-8](#).
- [67] B. J. Land, Z. Bagdasarian, J. Caravaca, M. Smiley, M. Yeh, G. D. Orebi Gann, MeV-scale performance of water-based and pure liquid scintillator detectors, *Phys. Rev. D* 103 (5) (2021) 052004. [arXiv:2007.14999](#), [doi:10.1103/PhysRevD.103.052004](#).
- [68] M. Askins, et al., Theia: Summary of physics program. Snowmass White Paper Submission, in: 2022 Snowmass Summer Study, 2022. [arXiv:2202.12839](#).
- [69] Y. Suzuki, The Super-Kamiokande experiment, *Eur. Phys. J. C* 79 (4) (2019) 298. [doi:10.1140/epjc/s10052-019-6796-2](#).
- [70] Y. Zhuang, L. E. Strigari, R. F. Lang, Time variation of the atmospheric neutrino flux at dark matter detectors, *Phys. Rev. D* 105 (4) (2022) 043001. [arXiv:2110.14723](#), [doi:10.1103/PhysRevD.105.043001](#).
- [71] A. Abusleme, et al., TAO Conceptual Design Report: A Precision Measurement of the Reactor Antineutrino Spectrum with Sub-percent Energy Resolution (5 2020). [arXiv:2005.08745](#).
- [72] Z. Xie, J. Cao, Y. Ding, M. Liu, X. Sun, W. Wang, Y. Xie, A liquid scintillator for a neutrino detector working at -50 degree, *Nucl. Instrum. Meth. A* 1009 (2021) 165459. [arXiv:2012.11883](#), [doi:10.1016/j.nima.2021.165459](#).

- [73] P. Adamson, et al., The MINOS scintillator calorimeter system, *IEEE Trans. Nucl. Sci.* 49 (2002) 861–863. doi:10.1109/TNS.2002.1039579.
- [74] D. S. Ayres, et al., The NOvA Technical Design Report (10 2007). doi:10.2172/935497.
- [75] M. Agostini, et al., Upgrade for Phase II of the Gerda experiment, *Eur. Phys. J. C* 78 (5) (2018) 388. arXiv:1711.01452, doi:10.1140/epjc/s10052-018-5812-2.
- [76] C. Buck, B. Gramlich, S. Schoppmann, Novel Opaque Scintillator for Neutrino Detection, *JINST* 14 (11) (2019) P11007. arXiv:1908.03334, doi:10.1088/1748-0221/14/11/P11007.
- [77] M. Auger, et al., The EXO-200 detector, part I: Detector design and construction, *JINST* 7 (2012) P05010. arXiv:1202.2192, doi:10.1088/1748-0221/7/05/P05010.
- [78] E. Aprile, H. Contreras, L. W. Goetzke, A. J. Melgarejo Fernandez, M. Messina, J. Naganoma, G. Plante, A. Rizzo, P. Shagin, R. Wall, Measurements of proportional scintillation and electron multiplication in liquid xenon using thin wires, *JINST* 9 (11) (2014) P11012. arXiv:1408.6206, doi:10.1088/1748-0221/9/11/P11012.
- [79] T. Ye, K. L. Giboni, X. Ji, Initial evaluation of proportional scintillation in liquid Xenon for direct dark matter detection, *JINST* 9 (12) (2014) P12007. doi:10.1088/1748-0221/9/12/P12007.
- [80] P. Juyal, K.-L. Giboni, X.-D. Ji, J.-L. Liu, On proportional scintillation in very large liquid xenon detectors, *Nucl. Sci. Tech.* 31 (9) (2020) 93. arXiv:1910.13160, doi:10.1007/s41365-020-00797-4.
- [81] P. A. Amaudruz, et al., Design and Construction of the DEAP-3600 Dark Matter Detector, *Astropart. Phys.* 108 (2019) 1–23. arXiv:1712.01982, doi:10.1016/j.astropartphys.2018.09.006.
- [82] A. Abusleme, et al., Radioactivity control strategy for the JUNO detector, *JHEP* 11 (2021) 102. arXiv:2107.03669, doi:10.1007/JHEP11(2021)102.
- [83] C. Cao, N. Li, X. Yang, J. Zhao, Y. Li, Z. Cai, L. Wen, X. Luo, Y. Heng, Y. Ding, A practical approach of high precision u and th concentration measurement in acrylic, *Nuclear Instruments and Methods in Physics Research Section A: Accelerators, Spectrometers, Detectors and Associated Equipment* 1004 (2021) 165377. doi:https://doi.org/10.1016/j.nima.2021.165377. URL https://www.sciencedirect.com/science/article/pii/S0168900221003612
- [84] L. Althüser, S. Lindemann, M. Murra, M. Schumann, C. Wittweg, C. Weinheimer, VUV Transmission of PTFE for Xenon-based Particle Detectors, *JINST* 15 (12) (2020) P12021. arXiv:2006.05827, doi:10.1088/1748-0221/15/12/P12021.
- [85] L. W. Kastens, S. B. Cahn, A. Manzur, D. N. McKinsey, Calibration of a Liquid Xenon Detector with Kr-83m, *Phys. Rev. C* 80 (2009) 045809. arXiv:0905.1766, doi:10.1103/PhysRevC.80.045809.
- [86] D. S. Akerib, et al., Tritium calibration of the LUX dark matter experiment, *Phys. Rev. D* 93 (7) (2016) 072009. arXiv:1512.03133, doi:10.1103/PhysRevD.93.072009.
- [87] E. Aprile, et al., Results from a Calibration of XENON100 Using a Source of Dissolved Radon-220, *Phys. Rev. D* 95 (7) (2017) 072008. arXiv:1611.03585, doi:10.1103/PhysRevD.95.072008.
- [88] W. Ma, et al., Internal calibration of the PandaX-II detector with radon gaseous sources, *JINST* 15 (12) (2020) P12038. arXiv:2006.09311, doi:10.1088/1748-0221/15/12/P12038.
- [89] D. Akerib, S. Alsum, H. Araújo, X. Bai, A. Bailey, J. Balajthy, P. Beltrame, E. Bernard, A. Bernstein, T. Biesiadzinski, et al., Low-energy (0.7-74 keV) nuclear recoil calibration of the lux dark matter experiment using dd neutron scattering kinematics, arXiv preprint arXiv:1608.05381 (2016).
- [90] E. Aprile, J. Aalbers, F. Agostini, M. Alfonsi, L. Althueser, F. Amaro, V. C. Antochi, F. Arneodo, L. Baudis, B. Bauermeister, et al., Xenon1t dark matter data analysis: Signal and background models and statistical inference, *Physical Review D* 99 (11) (2019) 112009.
- [91] L. Luo, et al., Improvement on the Linearity Response of PandaX-4T with new Photomultiplier Tubes Bases (12 2023). arXiv:2401.00373.
- [92] S. Sakamoto, T. Hasegawa, Y. Itow, S. Kazama, M. Kobayashi, M. Yamashita, Development of a low-noise SiPM for the DARWIN experiment, *PoS ICRC2023* (2023) 1435. doi:10.22323/1.444.1435.
- [93] P. Barrow, et al., Qualification Tests of the R11410-21 Photomultiplier Tubes for the XENON1T Detector, *JINST* 12 (01) (2017) P01024. arXiv:1609.01654, doi:10.1088/1748-0221/12/01/P01024.
- [94] C. He, et al., A 500 MS/s waveform digitizer for PandaX dark matter experiments, *Journal of Instrumentation* 16 (12) (2021) T12015. doi:10.1088/1748-0221/16/12/t12015. URL https://doi.org/10.1088/1748-0221/16/12/t12015
- [95] Y. Zhou, X. Chen, Data reduction strategy in the PandaX-4T experiment (11 2023). arXiv:2311.12412.

- [96] X. Wang, Z. Lei, Y. Ju, J. Liu, N. Zhou, Y. Chen, Z. Wang, X. Cui, Y. Meng, L. Zhao, Design, construction and commissioning of the PandaX-30T liquid xenon management system, JINST 18 (05) (2023) P05028. [arXiv:2301.06044](#), [doi:10.1088/1748-0221/18/05/P05028](#).
- [97] E. Aprile, et al., [The xenon1t dark matter experiment](#), The European Physical Journal C 77 (2017) 881. [doi:10.1140/epjc/s10052-017-5326-3](#).
URL <https://link.springer.com/article/10.1140/epjc/s10052-017-5326-3>
- [98] B. N. Inc. [\[link\]](#).
URL <https://barber-nichols.com>
- [99] H. Gong, K. L. Giboni, X. Ji, A. Tan, L. Zhao, The Cryogenic System for the Panda-X Dark Matter Search Experiment, JINST 8 (2013) P01002. [arXiv:1207.5100](#), [doi:10.1088/1748-0221/8/01/P01002](#).
- [100] L. Zhao, X. Cui, W. Ma, Y. Fan, K. Giboni, T. Zhang, J. Liu, X. Ji, The cryogenics and xenon handling system for the PandaX-4T experiment, JINST 16 (06) (2021) T06007. [arXiv:2012.10583](#), [doi:10.1088/1748-0221/16/06/T06007](#).
- [101] T. Zhang, J. Liu, et al., Thermal Management Design and Key Technology Validation for PandaX Underground Experiment [doi:10.48550/arXiv.2408.13433](#).
- [102] K. L. Giboni, P. Juyal, E. Aprile, Y. Zhang, J. Naganoma, A LN₂-based cooling system for a next-generation liquid xenon dark matter detector, Nucl. Sci. Tech. 31 (8) (2020) 76. [arXiv:1909.09698](#), [doi:10.1007/s41365-020-00786-7](#).
- [103] F. LePort, et al., A Magnetically-driven piston pump for ultra-clean applications, Rev. Sci. Instrum. 82 (2011) 105114. [arXiv:1104.5041](#), [doi:10.1063/1.3653391](#).
- [104] E. Brown, et al., Magnetically-coupled piston pump for high-purity gas applications, Eur. Phys. J. C 78 (7) (2018) 604. [arXiv:1803.08498](#), [doi:10.1140/epjc/s10052-018-6062-z](#).
- [105] E. Aprile, et al., Search for New Physics in Electronic Recoil Data from XENONnT, Phys. Rev. Lett. 129 (16) (2022) 161805. [arXiv:2207.11330](#), [doi:10.1103/PhysRevLett.129.161805](#).
- [106] G. Plante, E. Aprile, J. Howlett, Y. Zhang, Liquid-phase purification for multi-tonne xenon detectors, Eur. Phys. J. C 82 (10) (2022) 860. [arXiv:2205.07336](#), [doi:10.1140/epjc/s10052-022-10832-w](#).
- [107] Z. Wang, et al., [Large scale xenon purification using cryogenic distillation for dark matter detectors](#), Journal of Instrumentation 9 (2014) P11024. [doi:10.1088/1748-0221/9/11/P11024](#).
URL <https://iopscience.iop.org/article/10.1088/1748-0221/9/11/P11024>
- [108] X. Cui, et al., [Design and commissioning of the pandax-4t cryogenic distillation system for krypton and radon removal](#), Journal of Instrumentation 16 (2021) P07046. [doi:10.1088/1748-0221/16/07/P07046](#).
URL <https://iopscience.iop.org/article/10.1088/1748-0221/16/07/P07046>
- [109] R. Yan, et al., [Pandax-4t cryogenic distillation system for removing krypton from xenon](#), Review of Scientific Instruments 92 (2021) 123303. [doi:10.1063/5.0065154](#).
URL <https://pubs.aip.org/aip/rsi/article/92/12/123303/283310/PandaX-4T-cryogenic-distillation-system-for>
- [110] X. Cui, et al., [Radon removal commissioning of the pandax-4t cryogenic distillation system](#), Journal of Instrumentation 19 (2024) P07010. [doi:10.1088/1748-0221/19/07/P07010](#).
URL <https://iopscience.iop.org/article/10.1088/1748-0221/19/07/P07010>
- [111] E. Aprile, et al., [The xenon100 dark matter experiment](#), Astroparticle Physics, 2012, 35(9), 573-590 35 (9) (2012) 573–590. [doi:10.1016/j.astropartphys.2012.01.003](#).
URL <https://www.sciencedirect.com/science/article/pii/S0927650512000059>
- [112] N. Abgrall, et al., The Majorana Demonstrator radioassay program, Nucl. Instrum. Meth. A 828 (2016) 22–36. [arXiv:1601.03779](#), [doi:10.1016/j.nima.2016.04.070](#).
- [113] J. B. Albert, et al., [Investigation of radioactivity-induced backgrounds in exo-200](#), Phys. Rev. C 92 (2015) 015503. [doi:10.1103/PhysRevC.92.015503](#).
URL <https://link.aps.org/doi/10.1103/PhysRevC.92.015503>
- [114] R. Agnese, et al., [Projected sensitivity of the supercdms snolab experiment](#), Phys. Rev. D 95 (2017) 082002. [doi:10.1103/PhysRevD.95.082002](#).
URL <https://link.aps.org/doi/10.1103/PhysRevD.95.082002>
- [115] E. Aprile, et al., Double-Weak Decays of ¹²⁴Xe and ¹³⁶Xe in the XENON1T and XENONnT Experiments, Phys. Rev. C 106 (2) (2022) 024328. [arXiv:2205.04158](#), [doi:10.1103/PhysRevC.106.024328](#).

- [116] F. Agostini, et al., Sensitivity of the DARWIN observatory to the neutrinoless double beta decay of ^{136}Xe , *Eur. Phys. J. C* 80 (9) (2020) 808, [Erratum: *Eur. Phys. J. C.* 83, 996 (2023)]. [arXiv:2003.13407](#), [doi:10.1140/epjc/s10052-020-8196-z](#).
- [117] Z. Guo, et al., Muon flux measurement at China Jinping Underground Laboratory, *Chin. Phys. C* 45 (2) (2021) 025001. [arXiv:2007.15925](#), [doi:10.1088/1674-1137/abccae](#).
- [118] X. Chen, et al., **BambooMC — a Geant4 simulation program for the PandaX experiments**, *Journal of Instrumentation* 16 (09) (2021) T09004. [doi:10.1088/1748-0221/16/09/t09004](#). URL <http://dx.doi.org/10.1088/1748-0221/16/09/T09004>
- [119] D. G. Madland, E. D. Arthur, G. P. Estes, J. E. Stewart, M. Bozoian, R. T. Perry, T. A. Parish, T. H. Brown, T. R. England, W. B. Wilson, W. S. Charlton, **Sources 4a: A code for calculating (α, n), spontaneous fission, and delayed neutron sources and spectra** (9 1999). [doi:10.2172/15215](#). URL <https://www.osti.gov/biblio/15215>
- [120] Q. Wang, et al., An Improved Evaluation of the Neutron Background in the PandaX-II Experiment, *Sci. China Phys. Mech. Astron.* 63 (3) (2020) 231011. [arXiv:1907.00545](#), [doi:10.1007/s11433-019-9603-9](#).
- [121] X. Lu, et al., Measurement of solar pp neutrino flux using electron recoil data from PandaX-4T commissioning run*, *Chin. Phys. C* 48 (9) (2024) 091001. [arXiv:2401.07045](#), [doi:10.1088/1674-1137/ad582a](#).
- [122] M. Szydagis, N. Barry, K. Kazkaz, J. Mock, D. Stolp, M. Sweany, M. Tripathi, S. Uvarov, N. Walsh, M. Woods, **Nest: a comprehensive model for scintillation yield in liquid xenon**, *Journal of Instrumentation* 6 (10) (2011) P10002. [doi:10.1088/1748-0221/6/10/P10002](#). URL <https://dx.doi.org/10.1088/1748-0221/6/10/P10002>
- [123] M. Szydagis, J. Balajthy, J. Brodsky, J. Cutter, J. Huang, E. Kozlova, B. Lenardo, A. Manalaysay, D. McKinsey, M. Mooney, et al., Noble element simulation technique v2. 0, Zenodo: Geneve, Switzerland (2018).
- [124] N. Vinyoles, A. M. Serenelli, F. L. Villante, S. Basu, J. Bergström, M. C. Gonzalez-Garcia, M. Maltoni, C. Peña Garay, N. Song, A new Generation of Standard Solar Models, *Astrophys. J.* 835 (2) (2017) 202. [arXiv:1611.09867](#), [doi:10.3847/1538-4357/835/2/202](#).
- [125] J. Aalbers, S. AbdusSalam, K. Abe, V. Aerne, F. Agostini, S. A. Maouloud, D. Akerib, D. Y. Akimov, J. Akshat, A. Al Musalhi, et al., A next-generation liquid xenon observatory for dark matter and neutrino physics, *Journal of Physics G: Nuclear and Particle Physics* 50 (1) (2022) 013001.
- [126] C. Macolino, DARWIN: direct dark matter search with the ultimate detector, *J. Phys. Conf. Ser.* 1468 (1) (2020) 012068. [doi:10.1088/1742-6596/1468/1/012068](#).
- [127] D. Baxter, et al., Recommended conventions for reporting results from direct dark matter searches, *Eur. Phys. J. C* 81 (10) (2021) 907. [arXiv:2105.00599](#), [doi:10.1140/epjc/s10052-021-09655-y](#).
- [128] E. Bagnaschi, K. Sakurai, M. Borsato, O. Buchmueller, M. Citron, J. C. Costa, A. De Roeck, M. J. Dolan, J. R. Ellis, H. Flücher, S. Heinemeyer, M. Lucio, D. Martínez Santos, K. A. Olive, A. Richards, V. C. Spanos, I. Suárez Fernández, G. Weiglein, Likelihood analysis of the pMSSM11 in light of LHC 13-TeV data, *The European Physical Journal C* 78 (3) (Mar. 2018). [doi:10.1140/epjc/s10052-018-5697-0](#).
- [129] W. Ma, et al., Search for Solar B8 Neutrinos in the PandaX-4T Experiment Using Neutrino-Nucleus Coherent Scattering, *Phys. Rev. Lett.* 130 (2) (2023) 021802. [arXiv:2207.04883](#), [doi:10.1103/PhysRevLett.130.021802](#).
- [130] E. Aprile, et al., Dark Matter Search Results from a One Ton-Year Exposure of XENON1T, *Phys. Rev. Lett.* 121 (11) (2018) 111302. [arXiv:1805.12562](#), [doi:10.1103/PhysRevLett.121.111302](#).
- [131] D. S. Akerib, et al., Results from a search for dark matter in the complete LUX exposure, *Phys. Rev. Lett.* 118 (2) (2017) 021303. [arXiv:1608.07648](#), [doi:10.1103/PhysRevLett.118.021303](#).
- [132] E. Aprile, et al., Constraining the spin-dependent WIMP-nucleon cross sections with XENON1T, *Phys. Rev. Lett.* 122 (14) (2019) 141301. [arXiv:1902.03234](#), [doi:10.1103/PhysRevLett.122.141301](#).
- [133] D. S. Akerib, et al., Limits on spin-dependent WIMP-nucleon cross section obtained from the complete LUX exposure, *Phys. Rev. Lett.* 118 (25) (2017) 251302. [arXiv:1705.03380](#), [doi:10.1103/PhysRevLett.118.251302](#).
- [134] L. Baudis, DARWIN/XLZD: A future xenon observatory for dark matter and other rare interactions, *Nuclear Physics B* 1003 (2024) 116473, special Issue of Nobel Symposium 182 on Dark Matter. [doi:https://doi.org/10.1016/j.nuclphysb.2024.116473](#).

- [135] A. B. McDonald, Dark matter detection with liquid argon, *Nucl. Phys. B* 1003 (2024) 116436. [doi:10.1016/j.nuclphysb.2024.116436](https://doi.org/10.1016/j.nuclphysb.2024.116436).
- [136] M. J. Dolinski, A. W. P. Poon, W. Rodejohann, Neutrinoless Double-Beta Decay: Status and Prospects, *Ann. Rev. Nucl. Part. Sci.* 69 (2019) 219–251. [arXiv:1902.04097](https://arxiv.org/abs/1902.04097), [doi:10.1146/annurev-nucl-101918-023407](https://doi.org/10.1146/annurev-nucl-101918-023407).
- [137] S. Kumaran, L. Ludhova, O. Penek, G. Settanta, Borexino Results on Neutrinos from the Sun and Earth, *Universe* 7 (7) (2021) 231. [arXiv:2105.13858](https://arxiv.org/abs/2105.13858), [doi:10.3390/universe7070231](https://doi.org/10.3390/universe7070231).
- [138] B. Aharmim, S. Ahmed, A. Anthony, N. Barros, E. Beier, A. Bellerive, B. Beltran, M. Bergevin, S. Biller, K. Boudjemline, et al., Combined analysis of all three phases of solar neutrino data from the sudbury neutrino observatory, *Physical Review C* 88 (2) (2013) 025501.
- [139] N. Vinyoles, A. M. Serenelli, F. L. Villante, S. Basu, J. Bergström, M. Gonzalez-Garcia, M. Maltoni, C. Peña-Garay, N. Song, A new generation of standard solar models, *The Astrophysical Journal* 835 (2) (2017) 202.
- [140] M. Agostini, et al., Limiting neutrino magnetic moments with Borexino Phase-II solar neutrino data, *Phys. Rev. D* 96 (9) (2017) 091103. [doi:10.1103/PhysRevD.96.091103](https://doi.org/10.1103/PhysRevD.96.091103).
- [141] A. Beda, V. Brudanin, V. Egorov, D. Medvedev, V. Pogosov, E. Shevchik, M. Shirchenko, A. Starostin, I. Zhitnikov, Gemma experiment: The results of neutrino magnetic moment search, *Phys. Part. Nucl. Lett.* 10 (2013) 139–143. [doi:10.1134/S1547477113020027](https://doi.org/10.1134/S1547477113020027).
- [142] J. Aalbers, et al., Search for new physics in low-energy electron recoils from the first LZ exposure, *Phys. Rev. D* 108 (7) (2023) 072006. [arXiv:2307.15753](https://arxiv.org/abs/2307.15753), [doi:10.1103/PhysRevD.108.072006](https://doi.org/10.1103/PhysRevD.108.072006).
- [143] M. M. Miller Bertolami, Limits on the neutrino magnetic dipole moment from the luminosity function of hot white dwarfs, *Astron. Astrophys.* 562 (2014) A123. [doi:10.1051/0004-6361/201322641](https://doi.org/10.1051/0004-6361/201322641).
- [144] S. A. Díaz, K.-P. Schröder, K. Zuber, D. Jack, E. E. B. Barrios, Constraint on the axion-electron coupling constant and the neutrino magnetic dipole moment by using the tip-RGB luminosity of fifty globular clusters (10 2019). [arXiv:1910.10568](https://arxiv.org/abs/1910.10568).
- [145] A. Hitachi, T. Takahashi, N. Funayama, K. Masuda, J. Kikuchi, T. Doke, [Effect of ionization density on the time dependence of luminescence from liquid argon and xenon](https://arxiv.org/abs/1903.05279), *Phys. Rev. B* 27 (1983) 5279–5285. [doi:10.1103/PhysRevB.27.5279](https://doi.org/10.1103/PhysRevB.27.5279).
URL <https://link.aps.org/doi/10.1103/PhysRevB.27.5279>
- [146] D. S. Akerib, et al., Liquid xenon scintillation measurements and pulse shape discrimination in the LUX dark matter detector, *Phys. Rev. D* 97 (11) (2018) 112002. [arXiv:1802.06162](https://arxiv.org/abs/1802.06162), [doi:10.1103/PhysRevD.97.112002](https://doi.org/10.1103/PhysRevD.97.112002).
- [147] E. Hogenbirk, J. Aalbers, P. A. Breur, M. P. Decowski, K. van Teutem, A. P. Colijn, Precision measurements of the scintillation pulse shape for low-energy recoils in liquid xenon, *JINST* 13 (05) (2018) P05016. [arXiv:1803.07935](https://arxiv.org/abs/1803.07935), [doi:10.1088/1748-0221/13/05/P05016](https://doi.org/10.1088/1748-0221/13/05/P05016).
- [148] J. P. Brodsky, S. Sangiorgio, M. Heffner, T. Stiegler, Background Discrimination for Neutrinoless Double Beta Decay in Liquid Xenon Using Cherenkov Light, *Nucl. Instrum. Meth. A* 922 (2019) 76–83. [arXiv:1812.05694](https://arxiv.org/abs/1812.05694), [doi:10.1016/j.nima.2018.12.057](https://doi.org/10.1016/j.nima.2018.12.057).
- [149] M. Honda, M. Sajjad Athar, T. Kajita, K. Kasahara, S. Midorikawa, Atmospheric neutrino flux calculation using the NRLMSISE-00 atmospheric model, *Phys. Rev. D* 92 (2) (2015) 023004. [arXiv:1502.03916](https://arxiv.org/abs/1502.03916), [doi:10.1103/PhysRevD.92.023004](https://doi.org/10.1103/PhysRevD.92.023004).
- [150] Y. Suzuki, Low-energy solar neutrino detection by using liquid xenon, in: *Workshop on Solar Neutrinos below 1-MeV: NuLow, 2000*. [arXiv:hep-ph/0008296](https://arxiv.org/abs/hep-ph/0008296), [doi:10.1142/9789812778000_0009](https://doi.org/10.1142/9789812778000_0009).
- [151] M. Schumann, L. Baudis, L. Büttikofer, A. Kish, M. Selvi, Dark matter sensitivity of multi-ton liquid xenon detectors, *JCAP* 10 (2015) 016. [arXiv:1506.08309](https://arxiv.org/abs/1506.08309), [doi:10.1088/1475-7516/2015/10/016](https://doi.org/10.1088/1475-7516/2015/10/016).